Continental Shelf Research 205 (2020) 104165

Contents lists available at ScienceDirect

Continental Shelf Research

journal homepage: http://www.elsevier.com/locate/csr

The challenges of constraining shelf sea tidal models using seabed sediment grain size as a proxy for tidal currents

Sophie L. Ward [a,*], James D. Scourse [b], Yusuke Yokoyama [c], Simon P. Neill [a]

[a] School of Ocean Sciences, Bangor University, Menai Bridge, Isle of Anglesey, LL59 5AB, UK
[b] College of Life and Environmental Sciences, University of Exeter, Penryn Campus, Penryn, Cornwall, TR10 9EZ, UK
[c] Atmosphere and Ocean Research Institute, The University of Tokyo, Japan

ARTICLE INFO

Keywords:
Sediment transport
Palaeotidal model
ROMS
Glacial isostatic adjustment
Northwest European shelf seas
Last Glacial Maximum

ABSTRACT

Past major changes in sea level have had a significant influence on global- and shelf sea tidal dynamics. Some of these changes are preserved in sedimentary records from the shelf seas, and so appropriate proxy data have the potential to constrain tidal model outputs over the recent geological past. Tidal models which simulate the evolution of tide-dependent parameters over geological timescales are fundamental to understanding the response of the tides to sea-level rise and climate change. This study explores a potential new sedimentary proxy for validating past shelf sea tidal dynamics, interrogating the relationship between tidally-modulated bed shear stress and seabed sediment grain size at discrete sediment core locations over the northwest European shelf seas. Radiocarbon-dated sediment grain size profiles were generated for four British Geological Survey UK shelf sediment vibrocores, spanning a range of physical environments. Changes in observed sediment grain size through time were compared with simulated changes in tidal-induced bed shear through time, using temporal and spatial outputs from the most recently developed palaeotidal model of the Northwest European shelf seas. Although a positive correlation between observed grain size and simulated bed shear stress was observed at three of the four sediment cores sites, no robust relationship could be quantified. The palaeotidal model output failed to resolve the details of the actual sediment dynamics, since only tidal-induced bed shear stresses were considered. Wave processes were neglected, and the model was not sensitive enough to constrain simulated past tidal conditions at point locations; rather it is suitable for examining general trends. There remains a need to develop new proxies for past shelf sea hydrodynamic conditions which can be used to constrain numerical model output of tidal currents at regional scales.

1. Introduction

Glacio-eustatic sea level has risen by over 130 m since the Last Glacial Maximum (LGM) (Lambeck et al., 2002, 2004; 2010; Clark et al., 2009). The resultant flooding of shelf sea environments has had a major impact on a number of key Earth system attributes, including tidal dynamics (Belderson et al., 1986; Thomas and Sündermann, 1999; Uehara et al., 2002; Egbert et al., 2004; Hall and Davies, 2004; Neill et al., 2010; Scourse, 2013). Sediment dynamics over the northwest European shelf seas have been subject to considerable change over this time period due to these changes in tidal dynamics, with direct implications for basin and coastal evolution. Numerical models with realistic bathymetries and boundary conditions are a valuable tool for unravelling the complexity of how the main physical forcing mechanisms (e.g. tidal currents) have impacted the large-scale redistribution of sediments by shelf sea hydrodynamical processes.

The northwest European shelf (Fig. 1, inset) has demonstrated a complex isostatic response to deglaciation, and the British Isles themselves have been the focus of many studies of post-glacial isostatic adjustment (GIA) (e.g of Lambeck, 1993, 1995, 1996; Shennan et al., 2000; Peltier, 2002; Shennan et al., 2006; Bradley et al., 2011). Several palaeotidal modelling studies of the northwest European shelf seas have been conducted (Austin, 1991; Uehara et al., 2006; Neill et al., 2010; Ward et al., 2016). Palaeotidal model output can be applied to answer many questions including: for understanding the evolution of tidal dissipation through time and the resulting implications for the Earth-Moon system (Munk, 1997; Thomas and Sündermann, 1999; Green et al., 2009, 2017); for constraining sea-level index points (e.g.

* Corresponding author.
E-mail address: sophie.ward@bangor.ac.uk (S.L. Ward).

https://doi.org/10.1016/j.csr.2020.104165
Received 21 January 2019; Received in revised form 10 April 2020; Accepted 10 May 2020
Available online 24 June 2020

Ward et al., 2016), used as input to GIA models; and for assessing changes in the areal extent of the intertidal zone, with ecological, evolutionary and archaeological implications (Garrick-Bethell et al., 2006; Mortimer et al., 2013). To date, limited work has been invested in the 'validation' of palaeotidal model outputs, in which model outputs are constrained using observational data. Model validation through model-data comparison for past changes would provide an accurate constraint on the accuracy of these models, with implications for predictions of future changes. Austin and Scourse (1997) compared the Austin (1991) palaeotidal model outputs with faunal, isotopic and geochemical data from a single Celtic Sea (Fig. 1) sediment core in order to investigate the seasonal thermocline development in the region during the Holocene. The results of Austin and Scourse (1997) verified the model predictions of Austin (1991) for the position of the tidal mixing front in the Celtic Sea; however, no isostatic correction had been applied to the model palaeotopography of Austin (1991). The question of long-term dynamics of seasonal stratification was revisited by Scourse et al. (2002), who generated more extensive faunal datasets at the same core site, from the Late-glacial to the late Holocene (these data are used in this study). These palaeodata points were subsequently found to support the simulated timing of stratification onset in the Celtic Sea, from a revised palaeotidal simulation incorporating dynamic palaeotopography (Uehara et al., 2006). Clearly one data point for constraining regional palaeotidal models is insufficient, hence work is needed to find a proxy which can be applied at a regional scale to validate and constrain palaeotidal model output.

The shelf sea geological record registers multiple proxies which have the potential to be used to constrain palaeotidal models. The effects of tidal currents, waves, and wave-tide interaction can cause sediment transport through exerting a frictional force (referred to as the bed shear stress) on the seabed. Transport of (non-cohesive) sediments can occur when the currents are high enough for the bed shear stress to exceed the threshold of motion (Shields, 1936), which is dependent upon the median sediment grain size, d_{50} (Shields, 1936). Ward et al. (2015) discussed the relationship between simulated present-day tidal-induced bed shear stress and median grain size of seabed sediment grab samples, at a regional scale (Irish Sea, Fig. 1). The present day Irish Sea is tidally-dominated, although the relative contribution of tides and waves to sediment transport will have varied with sea-level rise since the LGM, with waves playing a relatively more significant role during times of lower sea levels than they do in the present day (Neill et al., 2010). Simulations by Neill et al. (2010) suggest that throughout the Holocene, in the northwest European shelf seas, the mean annual tidal-induced bed shear stress has been more significant than the mean annual wave-induced bed shear stress (see Fig. 6, Neill et al., 2010). Although simulation of the evolving wave climate is an interesting question which merits further attention, it is outside of the scope of the work presented here. Here, the aim was to explore whether observed stratigraphic grain size distributions from shelf sea sediment cores can be used as a proxy for past *tidal* current conditions, testing a novel method for validating a regional palaeotidal model using observations.

Sediment data for the Irish Sea, an energetic semi-enclosed sea, bordered by Ireland, Scotland, Wales and England (Section 2), were available from the British Geological Survey (BGS). We develop here new sediment grain size profiles for five BGS Irish Sea marine vibrocores, and age-constrain these results (Section 4.2) to generate an age-grain size evolution for each core, spanning *ca.* 13–2 ka BP. These grain size profiles are then considered alongside simulated bed shear

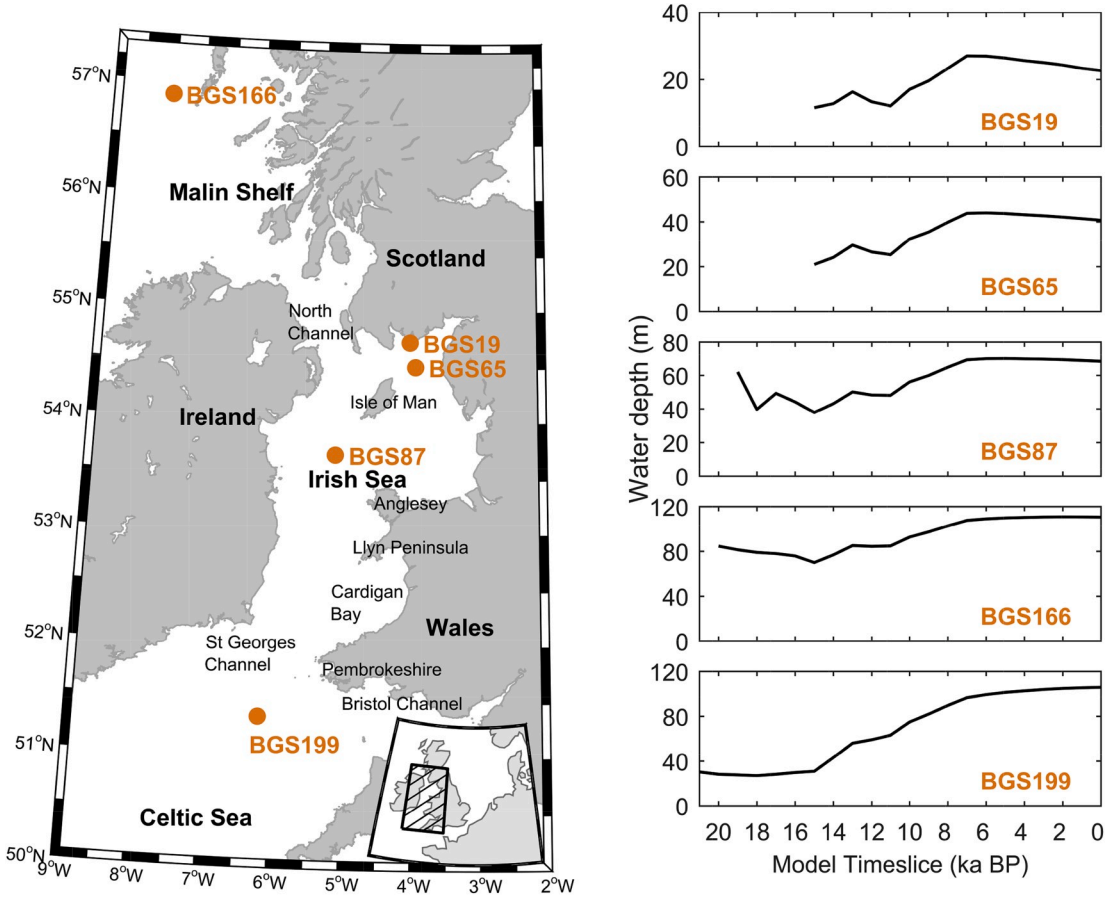

Fig. 1. Left panel: The Irish Sea and the marine sediment core locations used in this study (orange dots). Inset map: the position of the Irish Sea on the Northwest European Shelf. Right panels: water depths at the five BGS core sites at 1 ka time slices from 21 ka BP to present day, based on the palaeotopographies developed by Ward et al. (2016), incorporating the GIA model of Bradley et al. (2011).

stress evolutions at the core locations interpolated from the most recent palaeotidal model of the Northwest European shelf seas (Section 4.3). The aim was to investigate whether there is a robust relationship between temporal variations (over a long timescale) in observed seabed sediment grain size and simulated tidally-induced bed shear stress at the core sites.

2. The northwest European shelf, and the Irish and Celtic Seas

Due to the availability of geological data, and a well-developed palaeotidal model, the focus of this work is on the Irish Sea (Fig. 1). The present-day tides on the northwest European shelf are predominantly semi-diurnal (Pingree and Griffiths, 1978), dominated by the M_2 (lunar) and S_2 (solar) tidal constituents. Tidal energy propagates from the North Atlantic onto the shelf into the Celtic Sea. Some of the tidal wave propagates into the English Channel and through into the North Sea, while some passes into the Bristol Channel and into the Irish Sea (Pugh, 1987).

The deglaciation of the British-Irish and the Fennoscandian Ice Sheets, complete by 9 ka BP (Boulton et al., 1985; Scourse et al., 2009a), was a major source of sediment supply to the northwest European shelf seas, and played a significant role in the formation of large bedforms and in bathymetric evolution (Boulton et al., 1985; Neill et al., 2009, 2010; Scourse et al., 2009b). The glacial origin of northwest European shelf sea seabed sediments has led to the formation of a range of morphological features; a BGS map of present-day seabed sediments is reproduced in Ward et al. (2015). Morphological features in the Irish Sea include drumlins (e.g. Eyles and Marshall McCabe, 1989), large linear tidal sand ridges in the Celtic Sea (e.g. Scourse et al., 2009b, a; Lockhart et al., 2018), and evidence of ice streaming and calving in the Irish Sea (Van Landeghem et al., 2009). There is a significant diversity of present-day seabed sediment classifications within the Irish Sea itself, including areas of exposed bedrock (mostly limited to the northwest of Anglesey) and patches of semi-consolidated Pleistocene deposits, both covered in places only by thin transient patches of unconsolidated sediment. The majority of the seabed consists of sands and gravels, which are largely reworked glacial sediments. In the southern Irish Sea, sandy gravel is the predominant sediment type. Coarse sediments of glacial and glaciofluvial origin occupy both Cardigan Bay and St George's Channel. In the latter are several areas of exposed till, covered only by thin mobile sediment. Along the coast of Cardigan Bay is a belt of (mainly) sand, and the mud content increases towards the mouths of rivers. In the northern Irish Sea, there is a band of gravelly sediment to the south and north of the Isle of Man, which separates areas of muddy and sandy sediments to the east and west. West of the Isle of Man is a large area of mud, known as the Western Irish Sea Mud Belt, almost entirely surrounded by sandy mud, which itself is surrounded by muddy sand. Cohesive sediments in the Irish Sea are largely confined to the northwest Irish Sea Mudbelt and the Celtic Deep (e.g. Jackson et al., 1995).

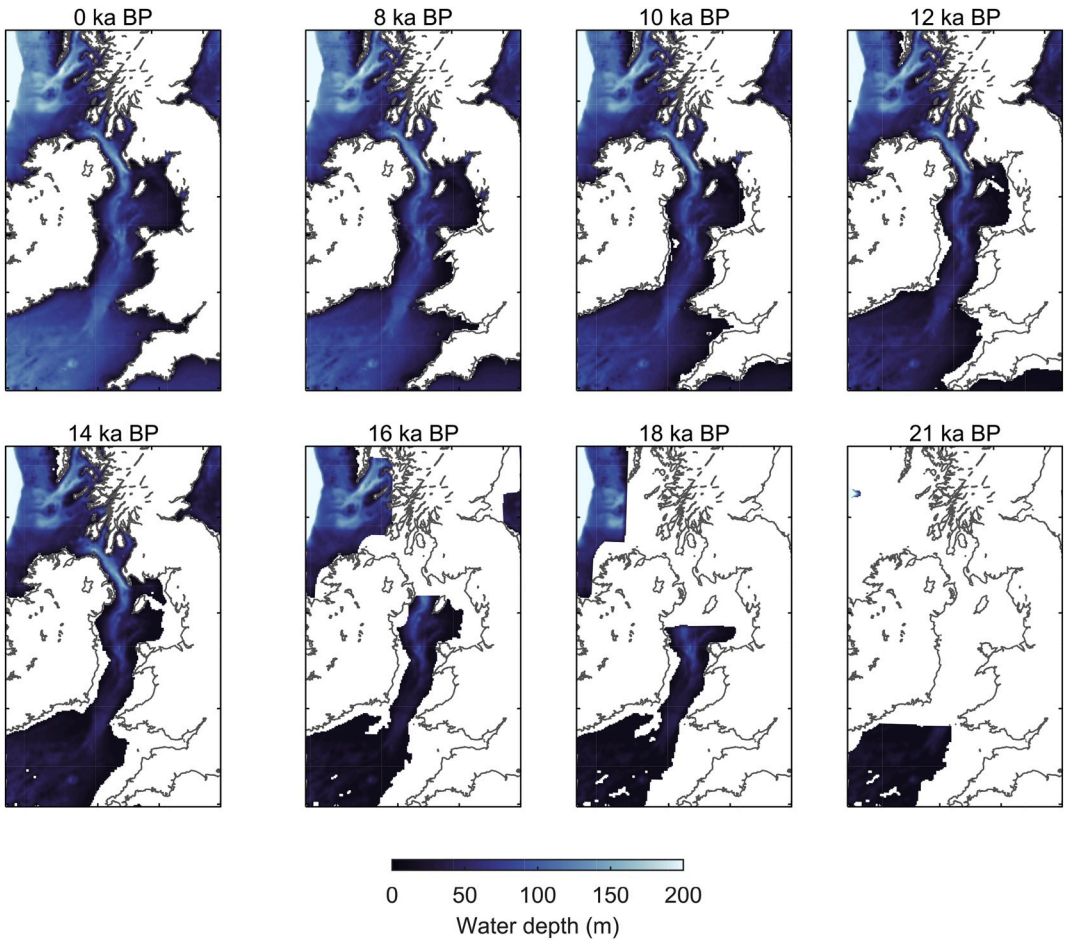

Fig. 2. Palaeobathymetries for selected time slices for the *ROMS + Bradley* palaeotidal model. The full shelf model (and hence the boundary conditions) extended further (see inset in Fig. 1, shown here is the same extent as the main panel in Fig. 1). The colour scale is set to a maximum water depth of 200 m to highlight the shelf seas. The white areas are land/ice, and the present-day coastline is provided for reference (grey line).

3. Methods

3.1. Tidal model

Here we describe the output from the high-resolution, three-dimensional, palaeotidal model of the northwest European shelf seas developed by Ward et al. (2016). The palaeotidal model, which is referred to here as *ROMS + Bradley*, was developed using the Regional Ocean Modeling system (ROMS, 1/24° longitude and variable latitudinal resolution of 1/34°–1/56° resulting in ~2–3 km grid). The model incorporated the GIA model of Bradley et al. (2011), combined with the present-day bathymetry derived from 1/120° GEBCO, to simulate the evolution of the tides in 1 ka increments from 21 ka BP (*ca.* since the LGM) to present day (Fig. 2). The model was forced at the boundaries using tidal elevation amplitudes and current velocities from the global palaeotidal model of Uehara et al. (2006). These simulations are compared with two-dimensional palaeotidal model simulations of Uehara et al. (2006) (referred to here as *KUTM + Lambeck*, KUTM being the Kyushu University Tidal Model), and a second three-dimensional ROMS palaeotidal model (*ROMS + Lambeck*), both of which incorporated a revised version of the GIA model of Lambeck (1995) into the palaeobathymetries. The focus here is on output of peak bed shear stress from the *ROMS + Bradley* model. Although the *ROMS + Bradley* and *ROMS + Lambeck* models were three-dimensional, the simulated depth-averaged peak bed shear stresses are used here for direct comparison with the earlier two-dimensional tidal model of Uehara et al. (2006).

3.2. Geological data: marine sediment cores

Here we consider five marine vibrocores, each collected and curated by the BGS (cores +54/-05/19, +54/-05/65, +53/-06/87, +56/-09/166, and +51/-07/199). The cores are referred to here as BGS19, BGS65, BGS87, BGS166 and BGS199 (Table 1). Since core selection was prior to the development of the tidal model of Ward et al. (2016), the core sites (Fig. 1) were selected based on the existing tidal model of past tidal conditions in the region, developed by Uehara et al. (2006). Regions on the shelf (and within the BGS geographical remit) which the simulations demonstrated to have considerable net change in bed shear stress from 21 ka BP–present day were identified, with the supposition that these regions were more likely to display significant variations in seabed sediment grain size through time than regions which had more moderate variations in tidal dynamics (and hence bed shear stress). All available BGS vibrocores within those identified regions were considered: all core logs were examined, and then a number of cores were visually inspected in the BGS archive. Core samples of less than 1 m in length were dismissed (as they were less likely than longer cores to hold a longer-term geological record), as were cores which displayed obvious evidence of bioturbation. Based on these criteria, five cores were selected and sampled (see Fig. 3 for lithostratigraphic logs).

Table 1
Details of the five BGS vibrocores.

Core	Latitude	Longitude	Water Depth (m)	Collection date	Core length (m)
BGS19	54°42.80'N	− 4°05.60' E	26	09/06/1969	6.10
BGS65	54°30.74'N	− 4°00.08' E	48	10/06/1969	6.10
BGS87	53°44.11'N	− 5°11.95' E	72	11/11/1980	5.93
BGS166	56°52.46'N	− 4°00.08' E	131	11/11/1985	3.71
BGS199	51°21.23'N	− 6°12.28' E	118	08/09/1982	5.68

Each core was sampled and particle size analysis was conducted using the Malvern Mastersizer 2000 laser particle diffractometer (size range 0.02–2000 μm). The grain size subsample positions were governed by several factors, including: the integrity of the cores; positions of previous samples; and visually-perceived changes in grain size. Between 17 and 25 samples were taken from each of the cores for laser particle analysis, and a total of 16 samples from BGS19/65/87/166 were analysed for AMS ^{14}C dating, with samples taken as near to the tops and bases of the cores as possible. BGS199 had an existing age-depth relationship, developed by Austin and Scourse (1997) and Scourse et al. (2002).

The results of the particle size analysis were post-processed using the GRADISTAT software (Blott and Pye, 2001), and the granulometric analysis used here for calculating the sample statistics was the graphical method of Folk and Ward (1957), which outputs statistics on sediment classification, including mean, mode, sorting and cumulative percentile values (e.g. d_{10}, d_{50} and d_{90}). The focus of this study was on the d_{50} (median grain size), as this is commonly used in sediment transport equations, such as in the Shields parameter (Shields, 1936) and in the Soulsby-Van Rijn formulation for total load (bedload plus suspended load) transport by waves and currents (Soulsby, 1997). Furthermore, d_{50} is a widely-recognised parameter for application of spatially-varying sediment classifications within hydrodynamic models, e.g. defining spatially-varying drag coefficients. Note that the method used here does not account for changes in sediment supply, and assumes that all sediment grain sizes have been available for resuspension and/or transport over the time period considered.

3.3. Radiocarbon dating

The complete AMS ^{14}C data (the existing dates for BGS199, plus 16 new samples from BGS19/65/87/166) are presented in Table 2. The dates are based on subtidal molluscs and benthic foraminifera. Though the species analysed have varying habitats (infaunal, epifaunal), comparative ^{14}C analyses demonstrate temporal offsets below the resolution required here (i.e. for comparison with 1 ka model timeslices) (see Scourse et al., 2002). The ^{14}C date ranges were output by the OxCal software (Bronk, 2013), where the calculations are based on the conventional radiocarbon age and the standard deviations ($\pm 1\sigma$) reported in the results from the laboratory analysis. The OxCal software (v4.2) uses the Intcal13 and Marine13 calibration curves of Reimer et al. (2013). The appropriate Marine Reservoir Corrections (ΔR) for each core (which varies by geographical location) were obtained using the 14CHRONO Marine Reservoir Effect database (Harkness, 1983; Butler et al., 2009), and were applied to the calibrated ages, resulting in the corrected, calibrated radiocarbon dates for each sample (cal BP).

4. Results

4.1. Sediment cores description

All of the marine sediment cores analysed here contained poorly- and/or very poorly-sorted sediment (mud and sand) throughout. Of note here is that in wave-dominated regions, sediments tend to be sorted by wave processes and fine sands and silts tend to be washed away (e.g. Anthony and Héquette, 2007). BGS19 was mud near the core bottom (5.2 m), and sandy mud from approximately 5 m core depth to the core top. BGS65 was mainly sandy mud throughout, with one facies of mud at around 1 m core depth. The sediment in BGS87 varied between sandy mud from 6-5 m core depth, and through (mainly) mud and sandy mud for 5-1 m core depth, up to muddy sand for the upper 1 m of the core. BGS199 was mud in the bottom of the core (5.3–4.7 m), coarser muddy sand for a section (4.7–3.3 m) and then sandy mud and mud to the core top. More extensive sediment grain size data are presented in Appendices A and B.

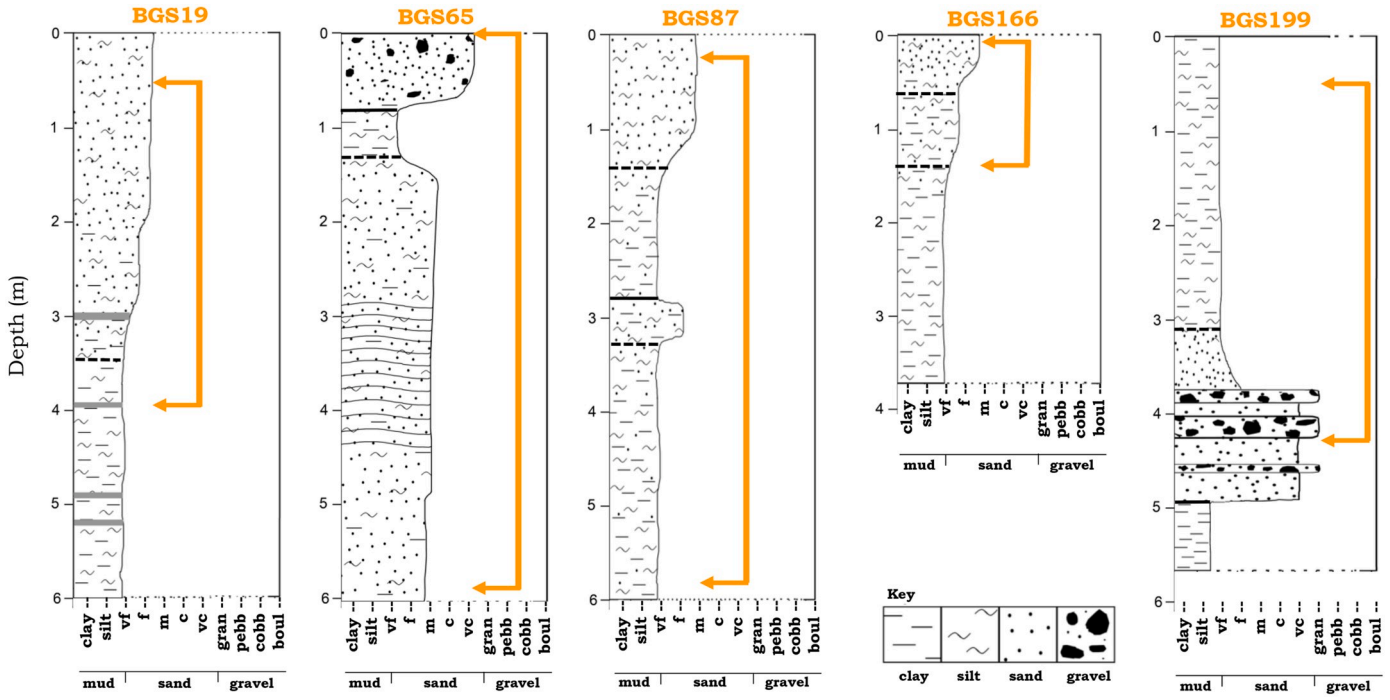

Fig. 3. Lithostratigraphic logs for vibrocores BGS19, BGS65, BGS87, BGS166 and BGS199. The horizontal lines on the logs indicate: gaps in the core record (grey), gradational contacts (black dashed), and abrupt contacts (solid black). The orange arrows indicate the dated extents of the cores.

Table 2
Radiocarbon dating results for BGS19, BGS65, BGS87, BGS166 and BGS199. Samples marked with a * were analysed at AORI, Japan, the remainder were analysed at the NERC Radiocarbon Dating Facility. Samples from BGS199 were dated previously (Austin and Scourse, 1997; Scourse et al., 2002). Where bivalve-foraminifera paired samples were taken, the selected date is in bold.

Core	Stratigraphic position (m down core)	d_{50} (μm)	Material	Sample weight (mg)	$\tilde{O}^{13}C_{PDB} \pm 0.1\%$	Conventional radiocarbon age (yr BP)	ΔR offset (years)	Calibrated age (cal BP) (Intcal13 and Marine13)
	0.49	53.43	*Ammonia batavus*	17.0	-0.2	1771 ± 37	-72	**1178-1325**
BGS19	0.49	53.43	*Venus casina*	58.5	0.2	2721 ± 41	-72	2246–2531
	3.18*	40.61	*Venus casina*	37.0	–	4630 ± 35	-72	4713–4885
	3.70*	15.69	*Corbula gibba*	7.5	–	5530 ± 30	-72	5772–5922
	3.93	13.31	*Corbula gibba*	18.1	1.5	6504 ± 38	-72	6830–7068
	0.00	151.97	*Corbula gibba*	19.8	1.4	7418 ±38	-72	7718–7888
BGS65	5.89	54.59	*Ammonia batavus*	5.9	-0.8	11938 ± 45	-72	**13207-13428**
	5.89	54.59	*Abra* sp.	3.0	-0.6	11511 ± 44	-72	12751-13054
	0.20	108.91	*Ammonia batavus*	5.5	-0.8	2981 ± 37	1	**2695-2841**
BGS87	0.20	108.91	*Abra prismatica*	6.3	0.4	477 ± 37	1	n/a-228
	0.79*	103.41	*Corbula gibba*	21.6	–	3600 ± 25	1	3408–3575
	1.32*	59.12	*Abra nitida*	8.2	–	4615 ± 30	1	4777–4942
	5.82	24.05	*Corbula gibba*	35.7	1.2	7871 ± 37	1	8236–8414
	0.01		*Cibicides* sp.	9.7	0.9	11865 ± 46	-29	13191-13416
BGS166	0.01		*Venus casina*	2.7	–	9842 ± 88	-29	10533-11021
	1.52		*Cibicides* sp.	11.6	0.9	11832 ± 46	-29	13161-13390
	0.50–0.51	9.89	*Bulimina marginata*		0.0	3010 ± 75	-15	2600–2978
BGS199	1.05–1.06	12.08	*Bulimina marginata*		0.1	3320 ± 50	-15	2999–3308
	1.55–1.56	18.40	*Bulimina marginata*		0.2	3765 ± 55	-15	3541–3837
	2.05–2.06	20.48	*Bulimina marginata*		-0.1	4675 ± 55	-15	4771–5055
	2.45–2.46	24.28	*Bulimina marginata*		0.0	5795 ± 60	-15	6020–6333
	2.75–2.76	13.82	*Bulimina marginata*		0.0	6210 ± 60	-15	6471–6788
	3.05–3.06	17.05	*Bulimina marginata, Quinqeloculina seminulum, Ammonia batavus*		0.0	7575 ± 70	-15	7881–8175
	3.35–3.36	157.37	*Quinqueloculina seminulum*		-0.1	8855 ± 115	-15	9252–9857
	4.20–4.30	272.26	*Spisula elliptica*		2.3	11570 ± 100	-15	12784-13253

4.2. Core age-depth relationships

The ^{14}C dates (Table 2) were used to generate age-depth relationships for each of the cores, which were then applied to the grain size profiles to display the evolution of grain size over time, rather than with core depth (Fig. 4 and Appendix B). The relationships are based on linear interpolation between the dated core depths, where the depths of the samples used in the model were taken to be the mid-point of the sample slices. The ^{14}C dating results for the upper and lower samples taken from BGS166 suggest significant reworking of the sample (*ca.* 13100–13400 cal BP for both 0.01 m and 1.63 m sample depths). An age-depth relationship for this core is thus not presented and BGS166 is not used for the model-data comparison in Section 4.3. In each of the three cases where paired datings of molluscs and foraminifera from the same level was carried out (BGS19 0.49 m sample depth, BGS65 5.89 m sample depth and BGS87 0.20 m sample depth), the dating results of the foraminifera samples have been used for the construction of the age-depth relationships. It was preferable to date a sample containing a number of *Ammonia batavus* over a single bivalve (or part of a bivalve), as these integrate any reworked specimens and reduce the possibility of a wholly erroneous date from a single bivalve or bivalve fragment as a result of bioturbation or reworking.

The analysed section of BGS19 was dated to between approximately 6900 and 2400 cal BP. The corresponding grain size profile (Fig. 4) from within this date range displayed a generally coarsening-upwards trend, remaining within the classification of silt (4–63 μm), with a slight inversion of the coarsening-upwards trend between 5000 and 3000 cal BP. The age-depth relationship for BGS65 is relatively crude, there being very few levels with suitable and sufficient material for dating. BGS65 was selected for analysis specifically because the grain size did not appear to change considerably upcore, ranging within the size classification for silt between 14000 and 8000 cal BP and thus there was no need to try and resolve specific features within the dated extent of the grain size profile. The age-constrained grain size profile for BGS87 displayed an overall coarsening upwards between *ca.* 8500 and 1500 cal BP, with median grain size variation within the silt fraction until a coarsening from silt to fine sand between 4500 and 3500 cal BP. The most interesting (dated) variation in grain size was in BGS199 (*ca.* 11000 to 3000 cal BP), which had the highest resolution age-depth relationship. The results from the particle size analysis showed a significant fining-upwards (from a fine-medium sand to a medium silt) until *ca.* 8000 cal BP, after which the grain size remained relatively constant.

4.3. Model-data comparison

For the most basic comparison, Fig. 5 indicates the correlations between observed median grain size and simulated bed shear stress at each core location (hereon, dates and timeslices are both referred to as 'ka BP'). Based on linear interpolation of sediment grain size within the dated extents of each core, where grain size was estimated at a position corresponding to a model timeslice (e.g. at 5000 ka BP ±100 years), the observed sediment grain size is plotted against simulated bed shear stress at that point in time from the core location within the tidal model domain (Fig. 5). The grain size profiles for the dated sections of the four cores were then compared directly with the simulated bed shear stress evolutions at the core sites (Fig. 6).

For BGS19, the correlation between the observed grain size and simulated bed shear stress is statistically highly significant, i.e. the r^2 value was greater than that for the 1% correlation coefficient for a sample size of 6 (Fig. 5). At the location of BGS19, there was an observed coarsening of core sediments, within the Wentworth silt classification, during which time there was a slight increase in simulated bed shear stress between *ca.* 7 and 2 ka BP (1.3–1.5 N m^{-2}). Of note here is that only small increases in simulated bed shear stress and coarsening of sediments were simulated/observed.

At core site BGS65, there was no statistically significant correlation between median sediment gain size and bed shear stress. From the bottom of the dated section of BGS65 (*ca.* 13 ka BP) to near the top of the core, (which was dated to *ca.* 8 ka BP), the median grain size fluctuated within the silt classification. There was an increase in observed median grain size, from silt to a fine sand (d_{50} of 150 μm), near the top of core

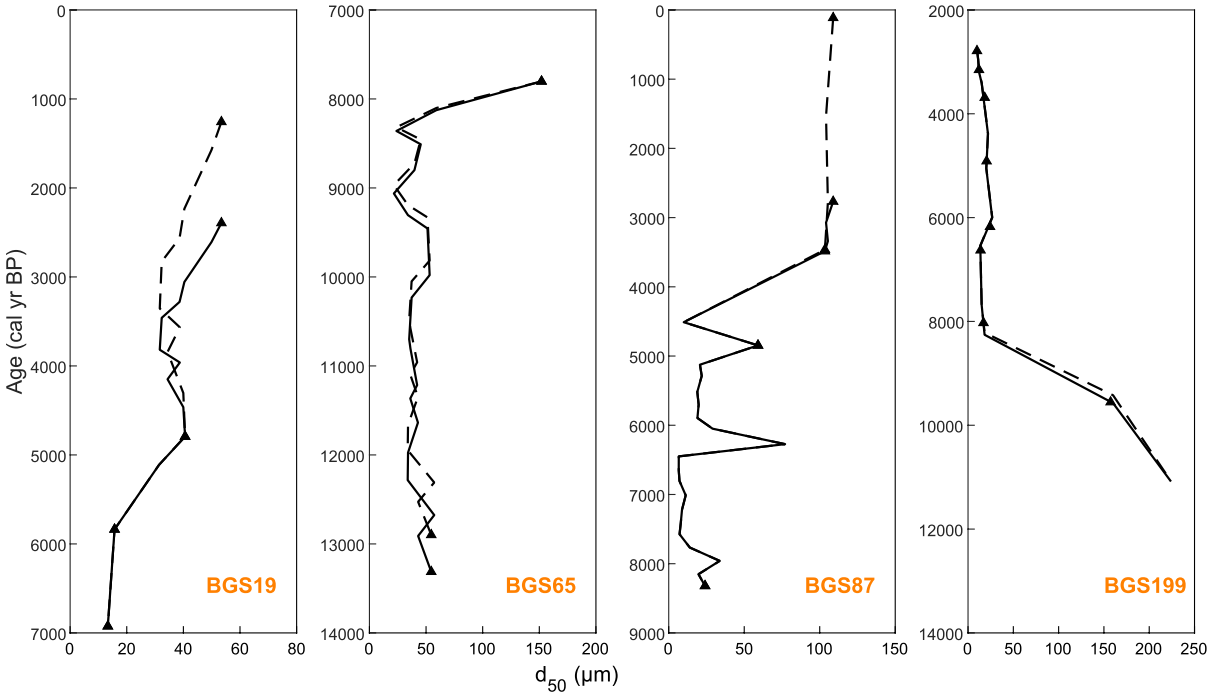

Fig. 4. Age-grain size evolutions for the four marine sediment cores, based on calibrated ages. Where different ages were obtained from samples at the same depths, the plots show the age-grain size profiles for both the preferred (solid lines) and discounted (dashed lines) samples. The triangle markers indicate the positions of ^{14}C samples. Note the varying scales.

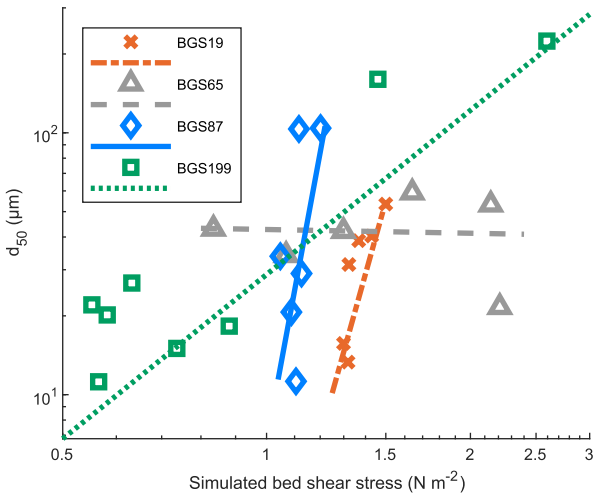

Fig. 5. Correlation between observed median grain size (d_{50}) from the dated extents of the four sediment cores and the modelled peak (maximum over a tidal cycle) bed shear stress at the core locations for the corresponding time slices. The R-squared values were $r^2 = 0.81$ (BGS19, n = 6), $r^2 = 0.003$ (BGS65, n = 6), $r^2 = 0.40$ (BGS87, n = 6) and $r^2 = 0.92$ (BGS199, n = 8). For reference, the critical correlation coefficient for the 5% coefficients are $r^2 = 0.5$ (n = 6) and $r^2 = 0.4$ (n = 8) and for the 1% coefficients are $r^2 = 0.7$ (n = 6) and $r^2 = 0.6$ (n = 8), respectively.

BGS65, where the coarsening of median grain size was observed in two samples. An increase in simulated bed shear stress at BGS65 occurred between 13 and 9 ka BP, which is earlier than the observed coarsening of sediments.

Although the correlation between the observed median grain size and simulated bed shear stress for the dated extent of BGS87 was not 'statistically significant' (i.e. $r^2 < 0.5$), Fig. 5 indicates a degree of positive correlation. The median grain size of BGS87 between *ca.* 8 and 3 ka BP (which was almost the entire length of the core) remained finer than a very fine sand (i.e. <125 μm), with no perceptible trend of coarsening- or fining-upwards of the median grain size. The variations in simulated bed shear stress within this period were small (between 1 and 1.2 N m^{-2}), with no significant increase or decrease between 8 and 3 ka BP.

As was found for BGS19, a 'highly significant' model-data correlation ($r^2 > 0.9$) was observed for the dated section of BGS199 (*ca.* 11 to 3 ka BP). A fining of median grain size was observed between *ca.* 11 ka BP (earliest dated section of the core) and 8 ka BP, from fine sand to silt, and the silt continued upwards through the remainder of the dated core section. There was a considerable reduction in simulated bed shear stress at this core location, from a peak of 7.5 N m^{-2} at 15 ka BP, to 2.6 N m^{-2} at 11 ka BP (start of the dated extent of the core), reducing further to 0.9 N m^{-2} by 8 ka BP (with a present-day value of 0.6 N m^{-2}).

5. Discussion

This is the first study that has investigated the relationship between changes in the sediment record (grain size) and tidal currents over a regional scale through time (LGM–present day). The basis for this is the assumption that at times of slower tidal current speeds, characterised by lower bed shear stresses, finer sediments are deposited in the geological record, whereas during times of higher current speeds, finer sediments remain in suspension whereas relatively coarser sediments can remain on the seabed (see Soulsby, 1997, for a detailed discussion of sediment transport by tidal currents). By considering the evolution of observed median grain size alongside corresponding changes in simulated bed shear stresses through time at four sediment core sites, we found no overall consistent statistically significant relationship.

With regards the three tidal models considered here (*ROMS + Bradley*, *ROMS + Lambeck* and *KUTM + Lambeck*), no single model set-up was found to have a consistently better fit with the trends in observed

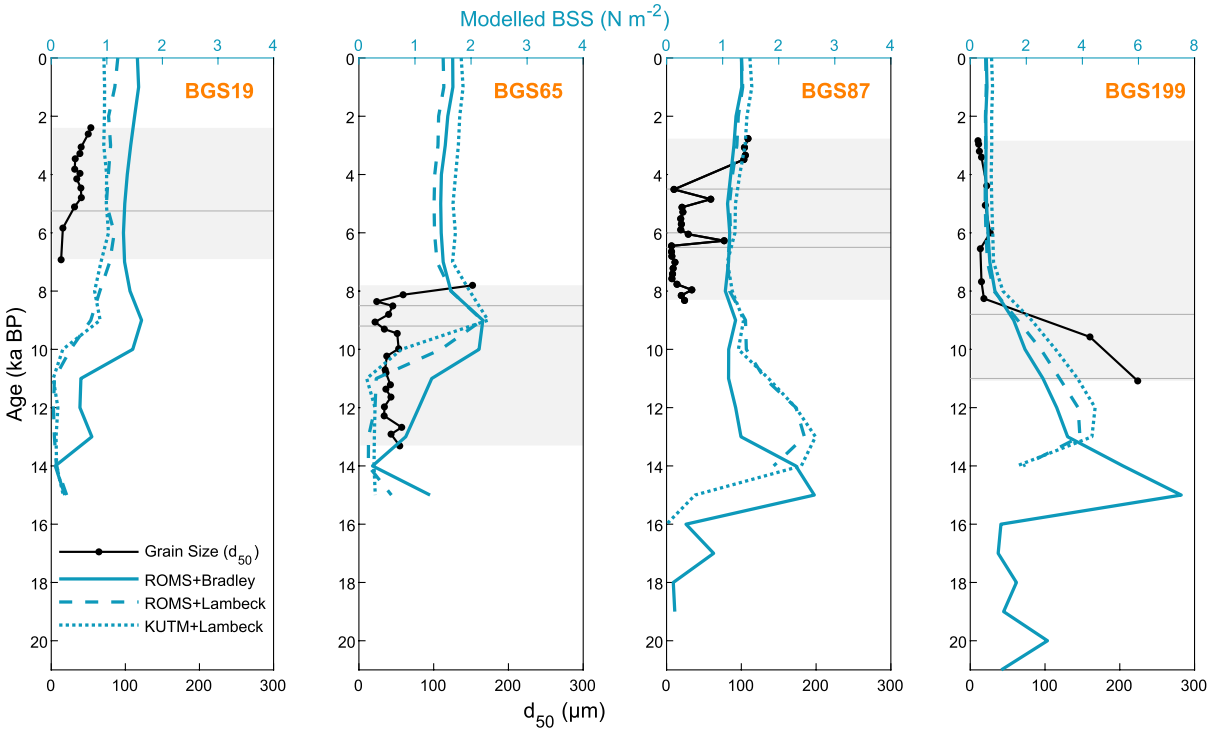

Fig. 6. Comparison of changes in simulated bed shear stress (blue lines, top x-axes, *ROMS + Bradley* = solid, *ROMS + Lambeck* = dashed, *KUTM + Lambeck* = dotted) at the core sites and observed median grain sizes (solid black lines, lower x-axes) within the dated extents of the cores (grey shading). The horizontal grey lines indicate the approximate position of contacts between lithological units, as given in Fig. 3. Note the different bed shear stress scale for BGS199.

changes in grain size. The timings of some of the major changes in bed shear stress (e.g. at locations of BGS87 and BGS199) varied between the tidal models, which reflects the differences in the GIA models (Lambeck, 1995; Bradley et al., 2011) used as input to the palaeotopographies of the tidal models. Because of the lack of quantifiable correlation between sediment grain size and bed shear stress found here, it is not possible to use these seabed sediment grain size data to 'validate' any particular tidal model. We therefore continue to focus the discussion on the *ROMS + Bradley* tidal model, since it is the most up-to-date and highest resolution palaeotidal model for the region. There are likely to be significant local variations in both hydrodynamic and sedimentological processes, which, because of the model grid resolution, the palaeotidal model output of bed shear stress cannot reproduce. To explore model-data uncertainty due to the nature of the point-source observational data vs. the gridded tidal model, a 'nearest-neighbour' approach was taken. Here we compared the bed shear stress output in the eight grid cells surrounding the model grid cell closest to the core location (Fig. 7). Consistently, in surrounding grid cells, similar trends in bed shear stress evolution were observed. The greatest *relative* variation in the magnitude of simulated bed shear stress in neighbouring grid cells was around core site BGS19, which is to be expected as it is the shallowest core site (present-day water depth of ~26 m), and so small changes in water depth can have a relatively greater influence on tidal dynamics than in deeper water.

Between 21 and 16 ka BP, the region with the highest bed shear stress was the shallow southwestern area of the shelf (the present day southern Celtic Sea) (Ward et al., 2016). This area of relatively high bed shear stress migrated northeast into the emerging English Channel, and subsequently northwards into the Irish Sea after the North Channel (Fig. 2) opened between 16 and 15 ka BP. Core site BGS199 is in deeper water than the other sites, and remained submerged since the LGM (see Fig. 1). The locations of BGS19, 65 and 87 were inundated (in this tidal model set-up) as the Irish Sea was inundated: at 19 ka BP (BGS87, which is further south) and at 15 ka BP (BGS19, 65), when tidal currents were not as energetic as at BGS199 (as indicated by the bed shear stresses in Fig. 7).

Of the four sediment cores considered, only BGS199 (from the Celtic Sea) was found to have a considerable change in grain size along the age-constrained (11–3 ka BP) length of the core (upwards-fining from fine sand to silt). The bed shear stress at BGS199 was also simulated to reduce over this time. It is possible that, had the dated section of the core extended further down the core, the trend of upwards-fining sediments may have started earlier, as suggested in Fig. 3, thus coinciding more closely with the simulated decreasing-upwards bed shear stress. BGS199 shows the greatest grain size variation, which is mirrored in the considerable decrease in modelled bed shear stress at the site prior to 8 ka BP. There has been ongoing relative sea-level rise at the site of BGS199 since 15 ka BP, whereas there has been a relative sea-level fall at each of the three other core sites since 7 ka BP. Some correlations were observed in the three Irish Sea cores (BGS19, 65 and 87), with coarser median grain sizes corresponding with higher simulated bed shear stress values although, on the whole, the fluctuations of observed median grain size were within one sediment size classification, e.g. silt, and variations in simulated bed shear stresses were small.

The difference between the age-depth models for BGS19 and BGS65 is interesting given their proximity to each other. Such a large difference between the sites is not seen in the model output of bed shear stress at the two sites. BGS65 is relatively poorly age-constrained, having only been dated at the core top and bottom, but the extent of BGS65 is older than the entire dated length of BGS19 (~4 m). Based on the radiocarbon age of the single mollusc sample (*Corbula gibba*), sedimentation at the location of BGS65 appears to have ceased over 7000 years ago. This apparently old surface sediment may be an indication of either deposition of a terrestrial source of ^{14}C known to influence radiocarbon ages in the area (Benoit et al., 1979), or due to reworking of older marine deposits (Kershaw, 1986). A further possibility is that there has been net erosion at this site since 7 ka BP, thus removing the sedimentary record, although this is unlikely given the minimal increase in modelled bed shear stress since 7 ka BP, and since the coastal embayments in the eastern Irish Sea have previously been considered to be acting as a sediment sink (Aston and Stanners, 1982; Kirby et al., 1983; Kershaw, 1986). It is possible that sediment transport at the site of BGS65 is not

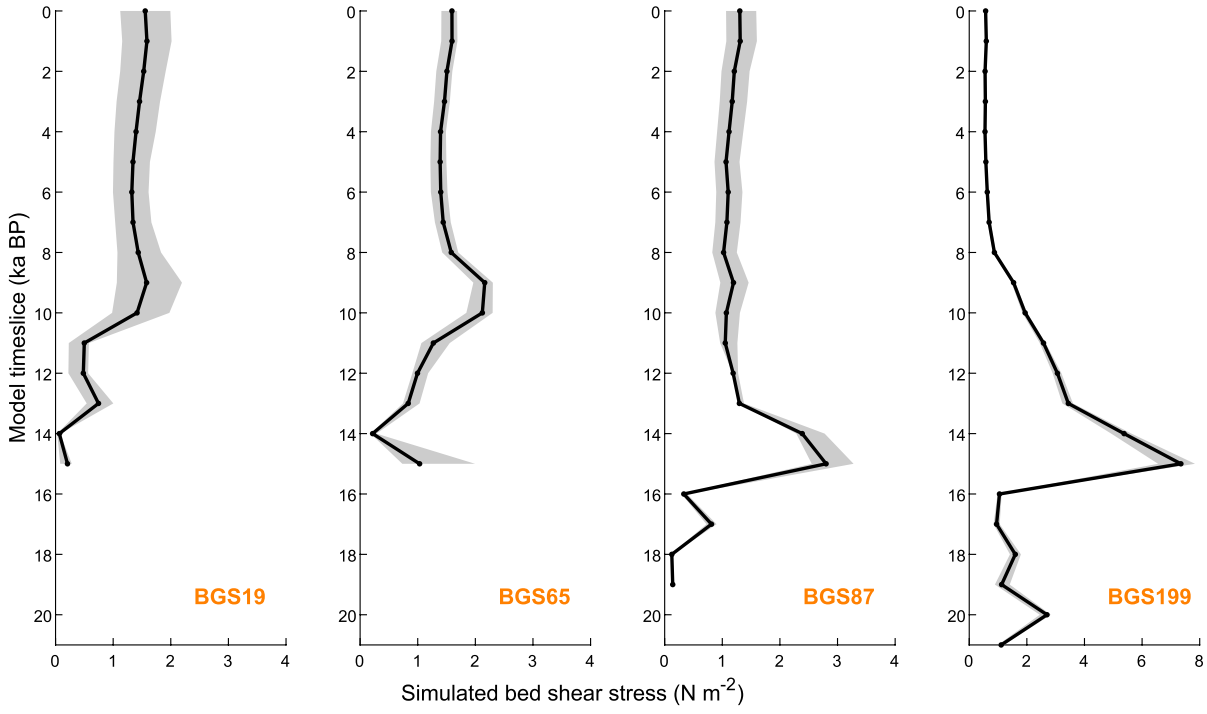

Fig. 7. Simulated peak bed shear stress evolution from *ROMS + Bradley* at the core sites (black lines) and in the eight model grid cells surrounding the core sites (grey lines).

tidally-dominated (i.e. that waves are important), or perhaps it is so close to the shore that consideration should be made for the sediment influx to the area.

Although tidal currents dominate shelf scale tidal currents (Pingree and Griffiths, 1979; Porter-Smith et al., 2004), waves also contribute to sediment transport, in particular in shallower regions of the shelf (e.g. van der Molen, 2002). It is likely that the shallower core sites considered here (e.g. BGS19, BGS65 and BGS87) will have experienced relatively greater wave-induced bed shear stresses than at the site of BGS199, in deeper water (see Fig. 1). In sufficiently shallow water, waves can produce an oscillatory velocity (and hence bed shear stress) at the seabed, which can act on seabed sediments. This wave-induced bed shear stress can be expected where 'sufficiently shallow water' is approximately $h < 0.1gT^2$, where h = water depth, g = acceleration due to gravity and T = wave period (Soulsby, 1997). In reality, during storm events, wave effects can reach the seabed over much of the continental shelf. By way of example, a surface wind wave of period 5 s could potentially exert a frictional force on the seabed in water depths < 24.5 m. Approximate annual (for 2014) mean wave periods at the cores sites have been calculated using model simulations presented in Roche et al. (2016) as: 4 s (BGS19 and BGS65), 5 s (BGS87) and 7 s (BGS199). Consideration of these mean wave periods alongside the evolution of water depths at the sites (Fig. 1) suggests that, within the period of dated sediment record for each site, none of the sites are in regions of consistent wave-induced bed shear stress. Of note here is that there is no consideration of palaeo-wave conditions. During times of transition from exposed site to submergence, the core sites are also likely to have been affected by wave effects due to breaking waves in the surf zone. Such transitions happened before the earliest dated sections of each core, i.e. are unlikely to be apparent in the geological records presented here.

The fine sediments in the core samples suggest that future investigations would benefit from further work on quantifying the relationship between simulated bed shear stress and both fine (cohesive) seabed sediments and mixed grain size beds. Mitchener and Torfs (1996) report a transition from non-cohesive to cohesive behaviour of sediments with mud content (by weight) between 3 and 15%. There was significant mud content in each of the cores, including in the top half of BGS199. The median grain sizes over much of the sediment core samples are <63 μm, indicating that at least 50% of these samples are in the mud range, and therefore possibly exhibit cohesive behaviour. This is likely to contribute to the mismatch between predicted and observed grain sizes in the core samples, since greater bed shear stresses would be needed to transport cohesive sediments than non-cohesive sediments of the same grain size. On this note, an improved understanding of the relationship between currents and various seabed sediment parameters (i.e. extending beyond d_{50}) would advance the implementation of spatially-varying drag coefficients in hydrodynamic models.

An important consideration is the degree to which the core data are representative of the dominant sediment type, or stratigraphy, in the areas from which they were collected. Overcoming this limitation would require extensive grain size and radiocarbon analysis of many more seabed sediment grab samples and marine sediment cores. Higher resolution age-depth relationships would constrain the sediment accumulation rates; however, AMS ^{14}C dates are expensive to produce. Deducing the depths to which mixing of the core sample (by either physical or biological processes) occurs is impossible without radiocarbon dating more material from additional sample depths. Many shelf sediment sequences from the region have been found to be heavily bioturbated (Kershaw et al., 1983; Scourse et al., 2002), which affects the age-depth profiles. There are inherent uncertainties linked to the linear-interpolation within the age-depth relationships, although it is a well-established method (e.g. Kershaw, 1986; Stuiver et al., 1998; Scourse et al., 2002; Blaauw, 2012). The method of linear interpolation omits any consideration of varying rates of deposition or erosion. In reality, temporal and spatial variations in deposition and erosion rates exist between dated depths, hence there may be hiatuses in the geological record which are not accounted for in the linear interpolation. Where turbulent mixing and bed shear stress are high, net sediment erosion is prone to occur in zones of flux divergence, thus producing gaps in the sediment record. Although this is important to note, there is no way to assess whether this has occurred in these sediment cores, or to quantify the extent to which it may have occurred. Further work is needed to understand small- and regional scale sedimentary processes, both for the present day and in the geological record, before grain size observational data can be used as reliable proxies for past hydrodynamic conditions.

6. Conclusions

Three new sediment core age-depth relationships (BGS19, BGS65 and BGS87) for locations in the Irish Sea complement the existing higher-resolution age-depth relationship developed by Austin and Scourse (1997) and Scourse et al. (2002) for BGS199, a vibrocore taken from the Celtic Deep. The four new age-grain size relationships developed here were fundamental to the comparison of observed seabed sediment grain size profiles and simulated bed shear stresses at the core locations (with focus on the period from the 21 ka BP to present day). Due to the complexity of sediment dynamics and limitations of the palaeotidal model, it was not possible to find a statistically-significant relationship between observed seabed sediment grain size and simulated bed shear stresses at the sediment core locations. The model-data relationship considered here is found to be unsuitable for constraining palaeotidal model simulations in this context. Future work should incorporate more extensive sediment data, and simulations should include both tide- and wave-induced bed shear stresses.

Declaration of competing interest

The authors declare that they have no known competing financial interests or personal relationships that could have appeared to influence the work reported in this paper.

Acknowledgements

Funding was provided by the Natural Environment Research Council (NERC) through grant NE/I527853/1 (Ph.D. studentship to SLW) and through Radiocarbon Analysis Allocation Number 1659.1012, with thanks to staff at the NERC Radiocarbon Laboratory. The authors acknowledge vital support from Peter Balson, and thank Peter and his colleagues at British Geological Survey for access to the marine vibrocores. The model simulations were undertaken on Supercomputing Wales, a collaboration between Welsh universities, the Welsh Government and the European Regional Development Fund (ERDF). The authors also thank an anonymous reviewer, alongside Alan Orpin (as well as two anonymous reviewers of an earlier version of the manuscript) for their comments and insight.

Appendix A. Supplementary data

Supplementary data to this article can be found online at https://doi.org/10.1016/j.csr.2020.104165.

References

Anthony, E.J., Héquette, A., 2007. The grain-size characterisation of coastal sand from the Somme estuary to Belgium: sediment sorting processes and mixing in a tide- and storm-dominated setting. Sediment. Geol. 202 (3), 369–382.

Aston, S.R., Stanners, D.A., 1982. The transport to and deposition of Americium in intertidal sediments of the Ravenglass Estuary and its relationship to Plutonium. Environ. Pollut. B Chem. Phys. 3 (1), 1–9.

Austin, R.M., 1991. Modelling Holocene tides on the NW European continental shelf. Terra. Nova 3, 276–288.
Austin, W.E.N., Scourse, J.D., 1997. Evolution of seasonal stratification in the Celtic Sea during the Holocene. J. Geol. Soc. 154 (2), 249–256.
Belderson, R., Pingree, R., Griffiths, D., 1986. Low sea-level tidal origin of Celtic Sea sand banks - evidence from numerical modelling of M2 tidal streams. Mar. Geol. 73, 99–108.
Benoit, G.J., Turekian, K.K., Benninger, L.K., 1979. Radiocarbon dating of a core from long Island sound. Estuar. Coast Mar. Sci. 9 (2), 171–180.
Blaauw, M., 2012. Out of tune: the dangers of aligning proxy archives. Quat. Sci. Rev. 36, 38–49.
Blott, S.J., Pye, K., 2001. GRADISTAT: a grain size distribution and statistics package for the analysis of unconsolidated sediments. Earth Surf. Process. Landforms 26, 1237–1248.
Boulton, G.S., Smith, G.D., Jones, A.S., Newsome, J., 1985. Glacial geology and glaciology of the last mid-latitude ice sheets. J. Geol. Soc. 142 (3), 447–474.
Bradley, S.L., Milne, G.A., Shennan, I., Edwards, R., 2011. An improved glacial isostatic adjustment model for the British Isles. J. Quat. Sci. 26 (5), 541–552.
Bronk, C., 2013. OxCal online. v4.2. http://c14.arch.ox.ac.uk/embed.php?File=oxcal.html.
Butler, P.G., Scourse, J.D., Richardson, C.A., Wanamaker, A.D., Bryant, C.L., Bennell, J. D., 2009. Continuous marine radiocarbon reservoir calibration and the 13C Suess effect in the Irish Sea: results from the first multi-centennial shell-based marine master chronology. Earth Planet Sci. Lett. 279, 230–241.
Clark, P.U., Dyke, A.S., Shakun, J.D., Carlson, A.E., Clark, J., Wohlfarth, B., Mitrovica, J. X., Hostetler, S.W., McCabe, A.M., 2009. The last glacial maximum. Science 325 (5941), 710–714.
Egbert, G.D., Richard, R.D., Bills, B.G., 2004. Numerical modeling of the global semidiurnal tide in the present day and in the last glacial maximum. J. Geophys. Res. 109 (C3), C03003.
Eyles, N., Marshall McCabe, A., 1989. The Late Devensian (22,000 BP) Irish Sea Basin: the sedimentary record of a collapsed ice sheet margin. Quat. Sci. Rev. 8 (4), 307–351.
Folk, R., Ward, W., 1957. Brazos River bar: a study in the significance of grain size parameters. J. Sediment. Petrol. 27, 3–26.
Garrick-Bethell, I., Wisdom, J., Zuber, M.T., 2006. Evidence for a past high-eccentricity lunar orbit. Science 313 (5787), 652–655.
Green, J.A.M., Green, C.L., Bigg, G.R., Rippeth, T.P., Scourse, J.D., Uehara, K., 2009. Tidal mixing and the meridional overturning circulation from the last glacial maximum. Geophys. Res. Lett. 36 (15), L15603.
Green, M., Huber, M., Waltham, D., Buzan, J., Wells, M., 2017. Explicitly modelled deep-time tidal dissipation and its implication for Lunar history. Earth Planet Sci. Lett. 461, 46–53.
Hall, P., Davies, A.M., 2004. Modelling tidally induced sediment-transport paths over the northwest European shelf: the influence of sea-level reduction. Ocean Dynam. 54 (2), 126–141.
Harkness, D.D., 1983. The extent of natural 14C deficiency in the coastal environment of the United Kingdon. In: Mook, W.G., Waterbolk, H.T. (Eds.), Proc. First Int. Symp. C-14 and Archaeology, vol. 8. PACT, pp. 351–364.
Jackson, D.I., Jackson, A.A., Evans, D., Wingfield, R.T.R., Barnes, R.P., Arthur, M.J., 1995. The Geology of the Irish Sea. Tech. Rep. British Geological Survey, London (HMSO).
Kershaw, P., 1986. Radiocarbon dating of Irish Sea sediments. Estuarine. Coast. Shelf Sci. 23 (3), 295–303.
Kershaw, P.J., Swift, D.J., Pentreath, R.J., Lovett, M.B., 1983. Plutonium redistribution by biological activity in Irish Sea sediments. Nature 306 (5945), 774–775.
Kirby, R., Parker, W., Pentreath, R., Lovett, M., 1983. Sedimentation studies relevant to low-level radioactive effluent dispersal in the Irish Sea. Part III. An evaluation of possible mechanisms for the incorporation of radionuclides into marine sediments. In: Tech. rep., Institute of Oceanographic Sciences Report, vol. 178 (Wormley, UK).
Lambeck, K., 1993. Glacial rebound of the British Isles-I. Preliminary model results. Geophys. J. Int. 115 (3), 941–959.
Lambeck, K., 1995. Late Devensian and Holocene shorelines of the British Isles and north sea from models of glacio-hydro-isostatic rebound. J. Geol. Soc. 152 (3), 437–448.
Lambeck, K., 1996. Glaciation and sea-level change for Ireland and the Irish sea since late Devensian/Midlandian time. J. Geol. Soc. 153 (6), 853–872.
Lambeck, K., Anzidei, M., Antonioli, F., Benini, A., Esposito, A., 2004. Sea level in Roman time in the Central Mediterranean and implications for recent change. Earth Planet Sci. Lett. 224 (3–4), 563–575.
Lambeck, K., Woodroffe, C.D., Antonioli, F., Anzidei, M., Gehrels, W.R., Jacques, L., Wright, A.J., 2010. Paleoenvironmental records, geophysical modeling, and reconstruction of sea-level trends and variability on centennial and longer timescales. In: Church, J.A., Woodworth, P.L., Aarup, T., Wilson, W.S. (Eds.), Understanding Sea-Level Rise and Variability. Wiley-Blackwell, Hoboken, NJ, USA, pp. 61–121. Ch. 4.
Lambeck, K., Yokoyama, Y., Purcell, T., 2002. Into and out of the last glacial maximum: sea-level change during oxygen isotope stages 3 and 2. Quat. Sci. Rev. 21 (1–3), 343–360.
Lockhart, E.A., Scourse, J.D., Praeg, D., Van Landeghem, K.J., Mellett, C., Saher, M., Callard, L., Chiverrell, R.C., Benetti, S., Cofaigh, C.Ó., Clark, C.D., 2018. A stratigraphic investigation of the Celtic Sea megaridges based on seismic and core data from the Irish-UK sectors. Quat. Sci. Rev. 198, 156–170.
Mitchener, H., Torfs, H., 1996. Erosion of mud/sand mixtures. Coast. Eng. 29 (1–2), 1–25.
Mortimer, T., Scourse, J., Ward, S., Uehara, K., 2013. Simulated Late-Glacial and Holocene Relative sea-level and palaeotidal changes on the Isles of Scilly: a new approach for assessing changes in the areal extent of the inter-tidal zone. Geosci. South-West Engl. 13 (2), 152–158.
Munk, W., 1997. Once again: once again—tidal friction. Prog. Oceanogr. 40 (1–4), 7–35.
Neill, S.P., Scourse, J.D., Bigg, G.R., Uehara, K., 2009. Changes in wave climate over the northwest European shelf seas during the last 12,000 years. J. Geophys. Res. 114 (C6), C06015.
Neill, S.P., Scourse, J.D., Uehara, K., 2010. Evolution of bed shear stress distribution over the northwest European shelf seas during the last 12,000 years. Ocean Dynam. 60, 1139–1156.
Peltier, W.R., 2002. On eustatic sea level history: last Glacial Maximum to Holocene. Quat. Sci. Rev. 21 (1–3), 377–396.
Pingree, R.D., Griffiths, D.K., 1978. Tidal fronts on the shelf seas around the British Isles. J. Geophys. Res. 83 (C9), 4615–4622.
Pingree, R.D., Griffiths, D.K., 1979. Sand transport paths around the British Isles resulting from M2 and M4 tidal interactions. J. Mar. Biol. Assoc. U. K. 59, 497–513.
Porter-Smith, R., Harris, P., Andersen, O., Coleman, R., Greenslade, D., Jenkins, C., 2004. Classification of the Australian continental shelf based on predicted sediment threshold exceedance from tidal currents and swell waves. Mar. Geol. 211 (1–2), 1–20.
Pugh, D.T., 1987. Tides, Surges and Mean Sea-Level - A Handbook for Engineers and Scientists. John Wiley & Sons, Ltd., Chichester.
Reimer, P.J., Bard, E., Bayliss, A., Beck, J.W., Blackwell, P.G., Bronk, C., Caitlin, R., Hai, E.B., Edwards, R.L., Friedrich, M., Grootes, P.M., Guilderson, T.P., Haflidason, H., Hajdas, I., Hatté, C., Heaton, T.J., Hoffman, D.L., Hogg, A.G., Hughen, K.A., Kaiser, K.F., Kromer, B., Manning, S.W., Niu, M., Reimer, R.W., Richards, D.A., Scott, E.M., Southon, J.R., Staff, R.A., Turney, C.S.M., van der Plicht, J., 2013. IntCal13 and Marine13 radiocarbon age calibration curves 0 - 50,000 years cal BP. Radiocarbon 55 (4).
Roche, R., Walker-Springett, K., Robins, P., Jones, J., Veneruso, G., Whitton, T., Piano, M., Ward, S., Duce, C., Waggitt, J., Walker-Springett, G., Neill, S., Lewis, M., King, J., 2016. Research priorities for assessing potential impacts of emerging marine renewable energy technologies: insights from developments in Wales (UK). Renew. Energy 99.
Scourse, J., 2013. Quaternary sea-level and palaeotidal changes: a review of impacts on, and responses of, the marine biosphere. Oceanogr. Mar. Biol. Annu. Rev. 51, 1–70.
Scourse, J.D., Austin, W.E.N., Long, B.T., Assinder, D.J., Huws, D., 2002. Holocene evolution of seasonal stratification in the Celtic Sea: refined age model, mixing depths and foraminiferal stratigraphy. Mar. Geol. 191 (3–4), 119–145.
Scourse, J.D., Haapaniemi, A.I., Colmenero-Hidalgo, E., Peck, V.L., Hall, I.R., Austin, W. E., Knutz, P.C., Zahn, R., 2009a. Growth, dynamics and deglaciation of the last British-Irish ice sheet: the deep-sea ice-rafted detritus record. Quat. Sci. Rev. 28 (27–28), 3066–3084.
Scourse, J.D., Uehara, K., Wainwright, A., 2009b. Celtic Sea linear tidal sand ridges, the Irish Sea Ice Stream and the Fleuve Manche: palaeotidal modelling of a transitional passive margin depositional system. Mar. Geol. 259 (1–4), 102–111.
Shennan, I., Hamilton, S., Hillier, C., Hunter, A., Woodall, R., Bradley, S., Milne, G., Brooks, A., Bassett, S., 2006. Relative sea-level observations in western Scotland since the Last Glacial Maximum for testing models of glacial isostatic land movements and ice-sheet reconstructions. J. Quat. Sci. 21 (6), 601–613.
Shennan, I., Lambeck, K., Horton, B., Innes, J., Lloyd, J., Mcarthur, J., Purcell, T., Rutherford, M., 2000. Late Devensian and Holocene records of relative sea-level changes in northwest Scotland and their implications for glacio-hydro-isostatic modelling. Quat. Sci. Rev. 19 (11), 1103–1135.
Shields, A., 1936. Application of similarity principles and turbulence research to bedload movement. In: Tech. rep., Hydrodynamics Laboratory. California Institute of Technology.
Soulsby, R.L., 1997. Dynamics of Marine Sand. Thomas Telford, London.
Stuiver, M., Reimer, P., Bard, E., Beck, J.W., Burr, G., Hughen, K.A., Kromer, B., McCormac, G., van der Plicht, J., Spurk, M., 1998. INTCAL98 radiocarbon age calibration, 24,000-0 cal BP. Radiocarbon 40 (3), 1041–1083.
Thomas, M., Sündermann, J., 1999. Tides and tidal torques of the world ocean since the Last Glacial Maximum. J. Geophys. Res. 104 (C2), 3159.
Uehara, K., Saito, Y., Hori, K., 2002. Paleotidal regime in the Changjiang (Yangtze) estuary, the east China sea, and the Yellow sea at 6 ka and 10 ka estimated from a numerical model. Mar. Geol. 183 (1–4), 179–192.
Uehara, K., Scourse, J.D., Horsburgh, K.J., Lambeck, K., Purcell, A.P., 2006. Tidal evolution of the northwest European shelf seas from the Last Glacial Maximum to the present. J. Geophys. Res. 111 (C9), C09025.
van der Molen, J., 2002. The influence of tides, wind and waves on the net sand transport in the North Sea. Continent. Shelf Res. 22 (18–19), 2739–2762.
Van Landeghem, K.J., Uehara, K., Wheeler, A.J., Mitchell, N.C., Scourse, J.D., 2009. Post-glacial sediment dynamics in the Irish Sea and sediment wave morphology: data-model comparisons. Continent. Shelf Res. 29 (14), 1723–1736.
Ward, S.L., Neill, S.P., Scourse, J.D., Bradley, S.L., Uehara, K., 2016. Sensitivity of palaeotidal models of the Northwest European shelf seas to glacial isostatic adjustment since the last glacial maximum. Quat. Sci. Rev. 151, 198–211.
Ward, S.L., Neill, S.P., Van Landeghem, K.J., Scourse, J.D., 2015. Classifying seabed sediment type using simulated tidal-induced bed shear stress. Mar. Geol. 367, 94–104.